Light propagation in a large volume liquid scintillator

February 23, 1999

Borexino Collaboration

G. Alimonti[g], C. Arpesella[a], M. Balata[a], G. Bellini[g], J. Benziger[l], S. Bonetti[g], B. Caccianiga[g], L. Cadonati[k], F.P. Calaprice[k], G. Cecchet[i], M. Chen[k], N. Darnton[k], A. de Bari[i], M. Deutsch[b], F. Elisei[j], F. von Feilitzsch[d], C. Galbiati[g], F. Gatti[e], M.G. Giammarchi[g], D. Giugni[g], T. Goldbrunner[d], A. Golubchikov[g], A. Goretti[g], T. Hagner[d], F.X. Hartmann[g], R. von Hentig[d], G. Heusser[f], A. Ianni[a], M. Johnson[l], M. Laubenstein[a], P. Lombardi[g], S. Magni[g], S. Malvezzi[g], J. Maneira[g,m], I. Manno[n], G. Manuzio[e], F. Masetti[j], U. Mazzucato[j], E. Meroni[g], M. Neff[d,o], L. Oberauer[d], A. Perotti[i], R.S. Raghavan[h], G. Ranucci[g], E. Resconi[a,p], C. Salvo[e], R. Scardaoni[g], S. Schönert[d], O. Smirnov[c], R. Tartaglia[a], G. Testera[e,*], R.B. Vogelaar[k,q], S. Vitale[e], O. Zaimidoroga[c].

a) Laboratori Nazionali del Gran Sasso - Assergi (Aq) - Italy
b) Massachusetts Inst. of Technology - Cambridge MA - USA
c) Joint Inst. for Nuclear Research - Dubna - Russia
d) Technical Univ. Munich - Garching - Germany
e) Physics Dept. of the University and INFN - Genova - Italy
f) Max-Planck-Institute fuer Kernphysik - Heidelberg - Germany
g) Physics Dept. of the University and INFN - Milano - Italy
h) Bell Laboratories - Murray Hill NJ- USA
i) Physics Dept. of the University and INFN - Pavia - Italy
j) Chemistry Dept. of the University and INFN - Perugia - Italy
k) Physics Dept. Princeton University - Princeton NJ - USA
l) Chemical Engineering Dept. Princeton University - Princeton NJ - USA
m) permanent address: Dep. de Física - Fac. de Ciências da Univ. de Lisboa - Portugal
n) Research Inst. for Part. and Nucl. Phys., - Budapest -Ungary
o) now at a)
p) now at e)
q) now at Virginia Politechnic Inst.- Virginia - USA

**) corresponding author: Dipartimento di Fisica Via Dodecanneso 33 16167 Genova -Italy; teleph. +39 (0)10 3536350; fax +39 (0)10 313358; e-mail testera@ge.infn.it*

PACS 07.77.Ka; 42.68.Ay; 14.60.Pq

Abstract

The fluorescence light propagation in a large volume detector based on organic liquid scintillators is discussed. In particular, the effects of the fluor radiative transport and solvent Rayleigh scattering are enphasized. These processes have been modelled by a ray-tracing Monte Carlo method and have been experimentally investigated in the Borexino prototype which was a 4.3 ton, 4π sensitive detector. The comparison between the model prediction and the experimental data shows a satisfactory agreement indicating that the main aspects of these processes are well understood. Some features of the experimental time response of the detector are still under study.

1 Introduction

The design of very large volume detectors based on organic liquid scintillators and the correct interpretation of the data obtained with such apparatus, require a detailed understanding of the optical properties of the scintillator and detailed models of the light emission process and of the light interaction inside the scintillator volume. While we focus our attention on the Borexino detector, the results discussed in this paper have a general validity. The Borexino detector for solar neutrinos [1] is based on the use of 300 tons of organic liquid scintillator, consisting of a binary mixture of pseudocumene (1,2,4-trimethylbenzene or PC) as solvent and PPO (2,5-diphenyloxazole) as primary fluor with a concentration of 1.5 g/l, contained inside a spherical 4.25 meters radius thin nylon bag. 2200 photomultipliers (PMTs) symmetrically mounted on a larger stainless steel sphere (13.5 meters diameter) surrounding the nylon bag, detect the scintillator light. The volume between the stainless steel sphere and the nylon bag will be filled by a buffer liquid consisting of Pseudocumene [2]. Borexino will detect scintillations due to the recoil electrons from the elastic scattering of neutrinos emitted in the radioactive decay of ^{7}Be in the sun. These electrons have a continuous energy spectrum extending from zero to 664 MeV and are expected to occur at a rate of 10 - 50 per day. The background rate due to radioactive contamination of the scintillator and its environment or to cosmic rays is expected to be at least of the same order of magnitude. Much of this background is eliminated by the use of three layers of "active" shielding of successively higher purity. The outermost is a 2.5 m thick water layer to absorb radioactive radiations from the experimental hall and identify cosmic ray events by Cherenkov radiation using a separate array of phototubes. The second is the PC buffer absorbing the radiations from contamination in the water, the steel sphere and the phototubes and also identifies high energy events, primarily by Cherenkov radiation. Finally, the outer 200 tons of the scintillator, the purest material in the detector absorbs radiations from the buffer.

Low rates and low energy are then the two characteristics of the expected events that impose very stringent constraints on the scintillator response and demand a detailed modelling of each phenomena influencing the light propagation. Both the number of detected photoelectrons and their time pattern are important elements in Borexino: the first one because it determines the energy resolution of the detector and the second one because it is one of the most powerful tool allowing the background reduction and identification. Buffer and scintillator are viewed by the same photomultipliers and the spatial separation of events from those in the inner 100 ton fiducial volume is based on the intensity and time distribution of the phototube pulses. Moreover, being the remaining background dominated by the intrinsic radioactivity of the scintillator, the pulse shape discrimination feature of the scintillator will be used to recognize the background α events. These considerations indicate that every phenomena influencing the light propagation and the time response of the detector has to be carefully taken into account.

The scintillator optical properties have been widely studied by using different techniques (ultraviolet and radiation excitation) on small scale samples (few cubic cm [3] [4]) and medium scale samples (about 10 liters [5], [6]). These measurements allowed a good characterization of various liquid scintillators mixtures suitable for Borexino and suggested the importance of two phenomena:

- the probability that the light absorbed by the scintillator fluor is reemitted;

- the light elastic scattering by the solvent.

As it will be clear in the following sections, the detector geometry and its dimensions are the key elements determining the real weight of these phenomena in the characteristics of the measured light output. The geometry of the laboratory setups and their dimensions were not suitable to completely quantify these effects. Here we report the results of the measurements on these subjects obtained by the Counting Test Facility detector (CTF) [7] [8] which is a Borexino prototype. Due to its quite large dimensions and, above all, to its 4π sensitivity, this detector offerred a unique instrument to single out and quantify the mentioned processes and to test in a 1/4 scale (linear) prototype the model calculation for Borexino.

2 Interaction of the emitted light with the fluor and the solvent

Charged particles loosing energy in the PC+PPO medium lead to the ionization and excitation mostly of the PC molecules which are present in larger quantities with respect to PPO ones. The PC excited molecules transfer their energy to the PPO ones and the radiative decay of the PPO excited molecules from the first excited state to the ground state is responsible for the observed fluorescence. The emission spectrum of the scintillator has been measured in front face geometry under ultraviolet excitation as described in [4] and is shown in fig. 1.

The concentration of PPO in PC has been optimized to obtain the maximum yield (that is a maximum energy transfer efficiency from PC to PPO) and the fastest time response to allow the scintillation event position reconstruction, while minimizing the PPO self absorption. Table 1 reports the time response data [3] of a small sample of the CTF mixtures measured for β and α excitation. The time decay of the emitted light is phenomenologically described by the sum of few exponentials having time constants τ_i:

$$S(t) = \sum_{i=1}^{N} \frac{q_i}{\tau_i} e^{-t/\tau_i} \tag{1}$$

(N=3 or 4). q_i is the fraction of the light emitted following the time behaviour e^{-t/τ_i}. As table 1 shows, the first exponential accounts for most of the emitted light. Note that the fastest τ_i value ($\tau_1 = 3.5 ns$) is only about two times higher than the intrinsic PPO light time decay, 1.6 ns. To improve the position resolution of the reconstructed scintillation event, it is important to have the shortest possible time decay.

The difference in the amount of light emitted at longer times for α and β events is the basis of the α-β discrimination capabability.

2.1 Radiative transport

The PPO light interacts both with the PC and the PPO molecules. The cross sections for these interactions have been obtained by usual ultraviolet spectroscopy methods, that is measuring the attenuation of a monocromatic light beam propagating along the x direction inside a scintillator sample. The results are described by the attenuation length $\Lambda(\lambda)$ at a given wavelength using the relation

$$I(x, \lambda) = I_0(\lambda) e^{-x/\Lambda(\lambda)} \tag{2}$$

where $I(x, \lambda)$ is the light intensity after a path x and $I_0(\lambda)$ is the intensity when $x = 0$. Fig. 2 shows the Λ values for pure PC and for PC with a PPO concentration of 1.5g/l. Note that the Λ values for interaction with PPO are very small for short wavelengths of the PPO emission spectrum; thus most of the interactions between photons and PPO happen very near to the primary scintillation point. The Λ values at higher wavelengths of the PPO emission spectrum, even if quite large, are not negligible in comparison with the Borexino scintillator dimensions.

The superposition between the PPO emission and absorption spectra, which is typical of many organic scintillators, is responsible for the process called sometimes radiation imprisonment (or radiative migration or radiative transport) [9] consisting in the absorption of a photon by the fluor molecula followed by a photon reemission. The reemitted photons have a random direction with respect to the primary one and the time scale for the reemission process is determined by the fluor light time decay. The reemission probability is equal to the quantum efficiency of the absorbing molecula which is around 0.8 for PPO. This absorption-reemission process could occur several times until either the photon escapes the scintillator volume or its wavelength falls in a region where the PPO absorption probability is negligible. Since the PPO absorption probability is much higher for the shortest λ of its spectrum than for the longest ones, the effect of successive absorption and reemission is the progressive shift of the PPO light toward the red side of its spectrum. This fact indicates (see also section 3) that most of the absorption and reemission processes happen close to the primary scintillation position.

2.2 Elastic scattering

From the comparison of the attenuation length of PC and PPO (fig. 2) it is evident that the interaction with the fluor is the most probable process for photons having wavelength less than about 360 nm while photons having higher λ values preferably interact with the solvent. It has to be noted that the band gap for the lowest-energy electronic transitions in the PC molecule is at 320 nm so the absorption of PC below 320 nm is strong. At wavelengths longer than 320 nm the absorbance of PC drops rapidly and the measured extinction coefficients roughly obey a λ^{-4} dependence, indicative of Rayleigh scattering. Rayleigh scattering refers to a process where the light is scattered elastically, without a change in wavelength. The cross section for Raylegh scattering by a gas molecule is easily related to the dipole polarizability of the molecule and shows the λ^{-4} dependence [10]. The magnitude of scattering by a liquid is one or two orders of magnitude less than predicted for a gas at that concentration being related to density fluctuations; however the dependence on the wavelength remains the same.

To confirm the hypothesis of the importance of the elastic scattering, the extinction coefficients reported in fig. 2 were compared with elastic scattering data obtained [11] by specrophotometric techniques and measuring the amount of light in a direction at an angle θ (usually $\theta = 90^0$) with respect to the primary light beam. (Elastically scattered photons are expected to have an angular distribution of the type $1 + cos^2(\theta)$)

The cross sections for elastic scattering and the corresponding attenuation lengths can be calculated from these data and table 2 shows the comparison between these results and the corresponding one (plotted in fig.2) obtained by the absorption measurements.

Clearly, if a photon is scattered out of the path in an absorption spectrophotometer, it is lost and such measurements cannot discriminate between absorption and elastic scattering. The lower attenuation lengths obtained by the absorption measurements at shorter wavelengths is expected because in that region there is still some absorption, in addition to scattering. The agreement between the two sets of data increases at longer wavelength indicating that the elastic scattering process is the dominant one in that wavelength region.

2.3 Effect on the detector response

The absorption and reemission mechanism and the elastic scattering influence the performances of the detector affecting various properties of the detected light (timing, global yield, spectrum) in a way which is strongly dependent on the detector dimensions and geometry. The degradation of the time response with increasing the detector dimensions and its link to the radiative transport process have been already envisaged by various authors [12] and experimentally investigated, [13] while different models have been proposed to describe the radiative transport [9]. For our purposes, not only the effect on the timing is important but also the influence of these processes on the total amount of detected light. Indeed as regards the radiative tranport, being the PPO quantum efficiency very high (0.8 as already mentioned) the probability of absorption by PPO without reemission is only 0.2 and this means that the amount of lost light (after interaction with PPO) in a detector having 4π sensitivity, like CTF or Borexino, is very low. This is because the reemitted photons have an uniform angular distribution and they will be collected by a spherically sensitive detector (with the only limit due to the geometrical coverage) while, on the other hand, they will be lost with high probability in apparatus measuring beam attenuation in one dimensional geometry or having a small acceptance angle. The same is true for the elastic scattering that leads to a loss of photons in a spectrophotometer but not in a detector like Borexino because it simply changes the photon flight direction. So, while from one hand, both the absorption reemission process and the elastic scattering cause a worsening of the scintillator time response (the first one because of the fluor light decay time and the second because it increases the spread in the trajectoy pathlengths) and thus they limit in principle the power of the timing measurement as a method to reconstruct the primary scintillation position in a large volume detector and the $\alpha - \beta$ discrimination efficiency, on the other hand the presence of these processes, instead of a simple absorption, results in a very small fraction of lost light in a detector having 4π simmetry and it makes the amount of collected light almost independent on the scintillation position.

3 Experimental data and comparison with Monte Carlo

The effects discussed in section 2 have been experimentally investigated in CTF, which was a Borexino protoyope. The CTF apparatus is widely described in [7]; here it is only necessary to recall that it consisted of a spherical nylon vessel having 1 meter radius filled with scintillator and immersed in ultrapure water. 100 PMTs mounted on six rings centered on the z axis surrounded the scintillator. As in Borexino, for every scintillation event where the number of hit PMTs is higher than a selected threshold, both the PMT charge and the arrival time of the first photoelectron on each PMT are recorded providing the measurement of the energy associated with the event and allowing its position reconstruction inside the nylon vessel.

The scintillator selected for most of the CTF runs was the PC+PPO mixture mentioned in the introduction.

The light propagation phenomena has been studied using data from standard CTF runs and a set of dedicated runs when radioactive sources were inserted in various positions inside the scintillator vessel. Monte Carlo simulations that modeled the propagation of scintillation light in CTF were developed: these were an important element in confirming the understanding of the physics of light propagation. Thus, measurements and modeling combine together to reveal and describe the non-trivial phenomenology of light propagation in large scintillator volumes. With this complete model, the simulations and extrapolations used to predict the light-collection performance of the Borexino detector are made reliable enough.

3.1 The Monte Carlo code

The Monte Carlo code consisted of ray-tracing algorithms: the simulation of a scintillation event begins by launching photons isotropically from their origin. In the simulation, the photons are assigned a wavelength, corresponding to the measured emission spectrum of PC or PPO, depending on the scintillating medium in which they were emitted. The photons are also assigned an emission time according the exponential-like time profile for scintillation light emission (see relation (1)). Throughout the tracking code, the wavelength and time were monitored for each photon.

The photons are traced in a geometry simulating the CTF detector until they either intersect a material boundary in the detector, or undergo an absorption or scattering interaction in the scintillator. In the former case, the photon undergoes reflection, refraction or absorption at the material interface and the algorithm continues to follow the new trajectory of the photon (if it is not absorbed). In the latter one an interaction takes place in the scintillating medium itself: in the CTF light-propagation model, the interaction probabilities at wavelengths longer than 320 nm were extracted from the extinction coefficient measurements in this spectral region. The interactions themselves were simulated as Rayleigh scattering. At shorter wavelengths the interaction was simulated as absorption by the PC molecule (with the absorption probabilities derived from the extinction coefficient measurements). In a similar way, for interactions with PPO, the transition wavelength between absorption and scattering was modeled at 400 nm and the probabilities were taken from the extinction coefficient measurements of PPO.
Absorption interactions in the scintillating media do not immediately terminate the tracking of the scintillation photons. The photons reemission by the excited molecula has been included in the model with reemission probability 0.8 for PPO and 0.34 for pure PC.
The reemitted fluorescence photons were modeled with an isotropic distribution and with an emission delay that followed the exponential fluorescence decay of the materials (τ = 1.6 ns for PPO and τ = 27 ns for pure PC). We assumed that the spectrum of the reemitted photons has the same shape as the primary one. This hypothesis is not true for all the organic molecules that could exhibit a red shift of their emission spectrum when excited at the long-wavelength edge of their absorption bands [14]. In

comparison, Rayleigh or elastic scattering was simulated with an angular distribution of $P(\theta) \propto (1 + \cos^2 \theta)$, with no effective time delay, and with no shift in the wavelength of the scattered photon.

As a final element in the scintillation light propagation model, the measured spectral response of the photomultipliers was included so that detected light could be converted into photoelectrons. At the photomultipliers, the water-glass interface was included in the simulations.

3.2 The window source in CTF center

The sources used in CTF consist of about $5ml$ volume quartz vial filled by PC+PPO (1.5g/l) and loaded by radon [15]. The ^{222}Rn decay chain has a distinctive signature in the coincidence $^{214}Bi -^{214} Po$: first a $\beta(+\gamma)$ decay with end point at 3.23 MeV, followed by a 7.688 MeV α decay with half life 164 μs. Due to the strong tag of the energy requirement of the α decay together with the time correlation of a previous β decay, it is efficient to discriminate this event from the background.

Clear evidence of the reemission and elastic scattering mechanisms comes from the comparison between the data obtained with "a full angle source" (omni source) and a " window source" placed in the detector center. An omni source is made by a quartz vial where the light can escape in all the directions and then illuminates all the photomultipliers with the same probability. A window source is obtained by darkening a fraction of the quartz surface in order to obtain emitted light only within a proper angle. Such kind of window source, directly illuminating only one half of the PMTs, has been inserted in the vessel filled by pure PC and in the vessel filled by PC+PPO allowing the possibility to distinguish between the PPO absorbtion/reemission and the PC elastic scattering contribution.

The mean photoelectron number seen by each PMT has been evaluated by fitting the charge spectrum for α signals of the ^{214}Po decay.

Photomultipliers lying in the detector dark side ideally detect only the light which is either absorbed/reemitted by the PPO or elastically scattered, while the PMT directly facing the window source detect both the light which did not interact and the one which underwent the described interactions.

Only a cluster of PMTs directly facing the window source and a cluster of PMTs exactly opposite to the first one have been taken into consideration to get rid of possible side effect of the source itself. Before each window source run, data with the omni source in the middle of the inner vessel have been collected in order to equalize any possible different light collection efficiency.

Calling Osc the light seen by the dark cluster in a window source run, the light seen by the cluster facing the source is the sum of $Osc + Dir$, where Dir is the direct light. The total light seen by a PM in real event 4π emission is $Tot = Dir + 2 * Osc$. The numbers R_{PC+PPO}, R_{PC} quoted below are the ratio between the absorbed/reemitted or elastically scattered light over the total light seen by a PMT in a real 4π emission event. The experimental results are

$$R_{PC+PPO} = \frac{2 * Osc}{Tot} = 0.44 \pm 0.02 \tag{3}$$

when the vessel has been filled by PC+PPO and

$$R_{PC} = \frac{2 * Osc}{Tot} = 0.2 \pm 0.01 \tag{4}$$

when the vessel has been filled by pure PC.

It should be emphasized that even without any interaction between the light and the scintillator molecula, the phototubes lying in the dark side would detect a signal because of the light reflection processes occurring on the nylon interface or on the photomultipliers glass. The results of relation (3) and (4) are obtained without any cut on the time distribution and so they take into account every reflection contribution that, as will be shown, are not relevant for this analysis.

The Monte Carlo code gives $R_{PC+PPO} = 0.48$ and $R_{PC} = 0.27$ with associated errors of the order of 10% mainly due to the approximations introduced in the model. Taking this into account, the agreement between Monte Carlo results and experimental data is satisfactory. The higher value obtained by the code for R_{PC} can be explained remembering that any interaction of a photon having λ higher than 320 nm is interpreted as elastic scattering while, as discussed in section (2.3), there could be still some absorption probability not completely negligible.

It is interesting to note that the code gives further results (in case of the vessel filled by PC+PPO) concerning the relative weight of the elastic scattering and radiative transport: in case of a 4π event in the detector center, the fraction of the detected photons that were only absorbed and reemitted by the PPO (but not elastically scattered) is 28%; the fraction of photons that are detected after some elastic scattering (but not a PPO reemission) is 11.1% while 8.9% of the detected photons experienced both the processes.

Fig. 3 shows the Monte Carlo distribution of the distances between the primary scintillation point and various positions where a PPO reemission occurs. As expected from the considerations of the previous section, most of the absorption and reemission processes happen very near to the primary scintillation position.

3.3 The omni source in CTF

Data were taken in CTF by moving the described omni source in various positions inside the scintillator vessel filled by PC+PPO. These data were first analyzed by looking only at the signals detected by the photomultipliers mounted on the top ring (z=2.47 m, assuming the inner vessel center at z=0). Fig. 4 shows the results together with the corresponding points obtained by the Monte Carlo code with various effects included. The figure shows that the long distance behaviour of the detected light is not reproduced by the absorption-reemission mechanism alone; the inclusion of reflection effects at the scintillator-nylon-water and water-PMT glass-photocathode interfaces improves the agreement between the data and the simulation at long distances, at the expense of shorter distances points. The complete propagation model, which includes also Raylegh scattering at long wavelengths gives the best reproduction of the experimental data. Note that in the data taken at z=-80 cm more light was observed than for z=-60 cm. This anomalous behaviour is possibly a manifestation of a lensing effect due to a non spherical vessel. Monte Carlo studies suggest the effect is due to light reflection on the local shape of the inner vessel. A similar qualitative behaviour of this experimental point has in fact been found looking at the photomultipliers in the opposite hemisphere even if the actual values are different.

The interesting effect is that these data show almost no light attenuation (the continuous line in fig. 4 represents the expected reduction in the light signal due only to the geometric solid angle effect). The importance of the CTF detector geometry in achieving this result can be understood comparing the result of fig. 4 with the total light intensity $\Phi(x)$ versus pathlength which can be calculated knowing the PPO emission spectrum, the PC and the PPO attenuation lengths by the relation

$$\Phi(x) = \int I_0(\lambda) \ \ e^{-x/\Lambda_{PC}(\lambda) - x/\Lambda_{PPO}(\lambda)} d\lambda \tag{5}$$

Relation (5) corresponds to what would be measured by an apparatus having a very small acceptance angle ("one dimension geometry") if every interaction between light and PPO or PC leads to a loss of photons from this acceptance angle. The result of the integral of (5) can be fitted by a two exponential law

$$\Phi(x) = N_0 * \left(a_1 e^{-x/l} + a_2 e^{-x/L}\right) \tag{6}$$

where $a_1 + a_2 = 1$ and $N_0 = \int I_0(\lambda) d\lambda$. In our conditions, $l \simeq 10cm$ is mostly due to the interaction with PPO and $L \simeq 3$ m is dominated by the effect of the interaction with PC. This type of light behaviour has been measured in a detector having a geometry different from the CTF but with similar photon pathlength. We refer to the test counter widely described in [5] and basically consisting of a cylinder (2 meters long, 8 cm diameter) filled by the scintillator and viewed by one photomultiplier (the same type used in CTF) at each end. Point like events can be generated in various positions along the tube axis by moving a radioactive source. The geometry and the optical properties of such apparatus make the photomultiplier acceptance independent on the scintillation position: thus a decrease in the number of photoelectrons detected by one PMT versus the scintillation position, means that some photons, while propagating from the production point to the counter end, leave the acceptance cone. The measured value of l and L are in agreement with those calculated using relation (2), and the Monte Carlo code, when applied to this geometry, reproduces the experimental result.

Light behaviours of this type have been found [16] also using other mixtures and experimental apparata having a geometry similar to that of [5].

The total number of photoelectrons detected in CTF with the source in various points shows a very small dependence on the primary scintillation position. By moving the source from top to bottom along the z axis of the vessel (about 2 meters path) the total number of detected photoelectrons changes only by a few percent. This uniformity in the amount of collected light is expected by our model; since the CTF radius is small in comparison with the mean value of the long distance effective attenuation length, $L \simeq 3m$, the sensitivity in verifying this fact is poor.

The comparison of the absolute numbers of the detected photoelectrons in CTF and in the cylindrical counter confirms that the lost light in CTF is a small fraction (around 20%). In fact:

1) the number of detected photoelectrons in the cylindrical counter at pathlength zero (N^0_{phe} of eqn (5)) is measured to be N^0_{phe}=10 phe/MeV. Clearly it is possible to write

$$N^0_{phe} = Y \quad \epsilon_{PMT} \quad G_{cyl} \tag{7}$$

where Y is the scintillator yield, ϵ_{PMT} is the efficiency of the PMT and $G_{cyl} = 5 \times\ 10^{-3}$ is the geometrical acceptance of the cylindrical counter.

2) the CTF energy calibration is obtained in an independent way as discussed in [8] and the result is that $N_{CTF} = 300 \pm 30$ photoelectrons/MeV are detected. Considering an event in the CTF center and calling P_{na} the probability that a photon is not lost we can

write

$$N_{CTF} \simeq Y \;\; \epsilon_{PMT} \;\; G_{CTF} \;\; P_{na} \tag{8}$$

where $G_{CTF} = 0.2$ is the geometrical CTF coverage.

3) relations (7) and (8) are consistent with the experimental numbers if $P_{na} \simeq 0.8$ which is what we expect from our model.

Note that the data allow the estimation of the scintillator absolute yield with an error around 10% as $Y = 11500 \;\; phe/MeV$ for β events having energy higher than few hundreds KeV.

3.4 Time response of the CTF detector

The study of the time distribution of the photelectron signals in CTF is another powerful tool to confirm the model describing the scintillator behaviour. Time distributions were generated by the Monte Carlo code and compared with the experimental data in various conditions. In CTF the arrival time of the first photoelectron to each PMT is recorded by a TDC having a range of ~ 120 ns.

Time distribution data referring to the window source immersed in the vessel filled by PC+PPO and the corresponding Monte Carlo predictions are shown in Fig. 5. The uppermost spectrum shows the time distribution of a PMT lying in the dark side of the detector while the other spectrum refers to the time data for a PMT directly illuminated. It can be noted that data (continuous line) and Monte Carlo plots (dotted line) are very similar and most of the real signal is well reproduced by our models. This "time" result together with the previous "charge" result show that the absorption, reemission and elastic scattering processes are reasonably understood and modelled. Nevertheless the experimental time distribution of the photomultiplier in the dark side is not completely reproduced by the Monte Carlo in the region around 10 ns (see fig.5) where the experimental spectrum shows a structure absent in the simulation. The interpretation of this effect requires further study.

In the dark PM data plot, a peak with about 30 ns delay with respect to the main peak is visible: this is the light reflection on the opposite side PMs typical for the CTF detector where the distance between opposite PMs is about 6 meters. This contribution is clearly a few percent effect that does not significantly affect this measurement. Finally, effects from reflection/refraction on the scintillator/nylon/water surfaces have been simulated and shown to be negligible for this purpose.

The time response of the detector has been studied not only for the source events but also for the standard CTF run data. The time information for a point-like scintillation event follows a distribution which is a convolution between the PMT time response and the scintillator one; the first parametrized with a gaussian (the transit time jitter distribution has a sigma equal to 1 ns), the second with the sum of two exponentials, one with a short, the other with a longeer decay time (see (1)). For a uniform distribution of events, the geometrical function has to be taken into account.

Fits were performed both to point-like source event distributions and to events uniformly distribuited in the scintillator vessel, e.g. ^{14}C in the scintillator. The first decay time component turned out to be $\sim$ 5 ns and the second component returned by the fit is $\sim$ 20 ns (see fig.6). The 5 ns fast decay time constant has to be compared with the 3.5 ns measured on the small sample laboratory test. This worsening of the scintillator time response is the expected effect of the PPO absorption-reemission process which shows up as an effective longer scintillator decay time. The comparison with the Monte Carlo time spectra shows that this 5 ns "effective short decay time" is reproduced by our calculation while the tail of the time spectra contains some unknown effect not included in our model. Indeed in the β data, the area under the second exponential is bigger than expected by approximately a factor of 3. The reason of this behaviour is still under study. It has to be pointed out that it cannot be explained with the effect of the elastic scattering that, in 1 m sphere, is limited to a few ns spread. The dependence on the volume and energy effects of light trapping due to total reflection and other phenomena affecting the light transport are still under study.

3.5 Reconstruction of the scintillation event positions

The space-time coordinates of the events are calculated from the PMT signal using a maximum likelihood method. The procedure is described in detail elsewhere [8]; we limit our considerations here to aspects connected with the scintillator modelling. The arrival time of each photon is $t_a = t_0 + t_d + t_f + t_j$ where t_0 is the event trigger time, t_d is the scintillator decay time, t_f is the photon time of flight and t_j is the PMT jitter. Once the calculated time of flight is subtracted, the quantity

$$t_d + t_j = t_a - t_0 - t_f \tag{9}$$

is independent of the event position. After all the scintillator measurements were made, a good understanding of the fast component of the scintillation decay time (delayed photons, having potentially lost the production point information after multiple interactions and reflections, are discarded in the event reconstruction by a time cut) was reached, which allowed us to use the probability density function $p(t_d + t_j)$ inferred from the Monte Carlo. Checks with the Rn-source of known position were performed: the nominal values are reconstructed within a few cm error. The spatial resolution for ^{214}Po (see fig. 7) events was found to vary from approximately $\sim$ 12 cm in the inner region to $\sim$ 15 cm close to the vessel walls where more complicated phenomena at the different medium interface may occur (e.g total reflection) causing a loss in the light yield.

4 Conclusions

The results described in this paper show that the main processes influencing the light propagation in a large volume organic liquid scintillator are reasonably understood and modelled. The fluor absorption and reemission and the solvent elastic scattering determine the main features of the detector response. Their importance, together with the effects related to the detector geometry, have been clearly singled out. Even if the present work deals specifically with the PC+PPO mixture, the interpretation of the experimental results and their statistical modelling can be applied to liquid mixtures of organic scintillators in general.

Some features of the time response of the CTF detector are not completely described yet by the discussed model: these effects are still under study.

Table captions

TABLE 1

Scintillator light time decay

TABLE 2

Absorption data and elastic scattering data: comparison

Figure captions

Figure 1:

PC+PPO(1.5 g/l) emission spectrum

Figure 2:

Attenuation length of PC and PPO(1.5 g/l) calculated from the measured extinction coefficients.

Figure 3:

Simulation of an event corresponding to 1 MeV energy in the detector center: distribution of the reemission points.

Figure 4:

Omni source: light detected by the uppermost PMT in CTF and compariosn with the Montecarlo data.

Figure 5:

Window source in PC+PPO: time distribution measured by a PMT in the dark detector side (upper plot) and by a PMT directly illuminated (lower plot)

Figure 6:

Time distribution for β particles. P1 and P2 are respectively the mean value and the sigma value of the gaussian curve, P4 and P6 are the two exponential time constant (ns) while P3 and P5 are their weights.

Figure 7:

Space resolution.

Table 1: *Scintillator light time decay*

excit. type	$\tau_1(ns)$	$\tau_2(ns)$	$\tau_3(ns)$	$\tau_4(ns)$	q_1	q_2	q_3	q_4
β	3.57	17.61	59.50		0.895	0.063	0.042	
α	3.25	13.49	59.95	279.1	0.630	0.178	0.119	0.073

Table 2: *Absorption data and elastic scattering data: comparison*

$\lambda(nm)$	$\Lambda_{ass}(m)$	$\Lambda_{scatt}(m)$
340	3.1	1.6
360	3.5	2.8
380	5.1	4.1
400	5.7	5.2
420	7.8	6.6
436	8.3	8.2
460	8.2	11.1

References

[1] C. Arpesella et al.,*"Borexino at Gran Sasso: proposal for a real time detector for low energy solar neutrinos"* , Milano (1991); G. P. Bellini, Nuclear Physics B (Proc. Suppl.) 48 (1996) 363; M. Giammarchi, Int. Symp. on Lepton and Baryon number violation, Trento, Italy (1998) to be published

[2] M. Chen, F. Elisei, F. Masetti, U. Mazzucato, C. Salvo, G. Testera, NIM A 420 (1999) 189

[3] G. Ranucci et al., NIM A 350 (1994) 338

[4] F. Masetti F. Elisei, U. Mazzucato, J. Lumin. 68 (1996) 15

[5] F. Gatti, G. Morelli, G. Testera, S. Vitale, NIM A 370 (1996) 609

[6] F. Elisei et al., NIM A 400 (1997) 53

[7] G. Alimonti et al. (Borexino collaboration) NIM A 406 (1998) 411

[8] G. Alimonti et al. (Borexino collaboration) Astrop. Physics 8 (1998) 141

[9] M. N. Berberan-Santos et al.,J. Chem. Phys. 8 (1995) 3022; J. M. Martinho, J. Chem. Phys. 90 (1) (1989) 53

[10] M. Kerker "The scattering of light and other electromagnetic radiation" 1969 Academic Press (London)

[11] M. C. Johnson, Borexino internal report (1996)

[12] S. L. Prunty, NIM A245 (1986) 563; B. Sipp et al.,NIM A 114 (1974) 255

[13] P. Wiorkowski, Optics Comm. 53,2 (1985) 217; M. Braun et al., Optics Comm. 53,4 (1985) 221

[14] K. A. Al-Hassan et al., Chem. Phys. Letters 123 (1986) 39

[15] M. Johnson et al., NIM A 414 (1988) 459

[16] Macro collaboration, INFN/AE 96-22 (1996)

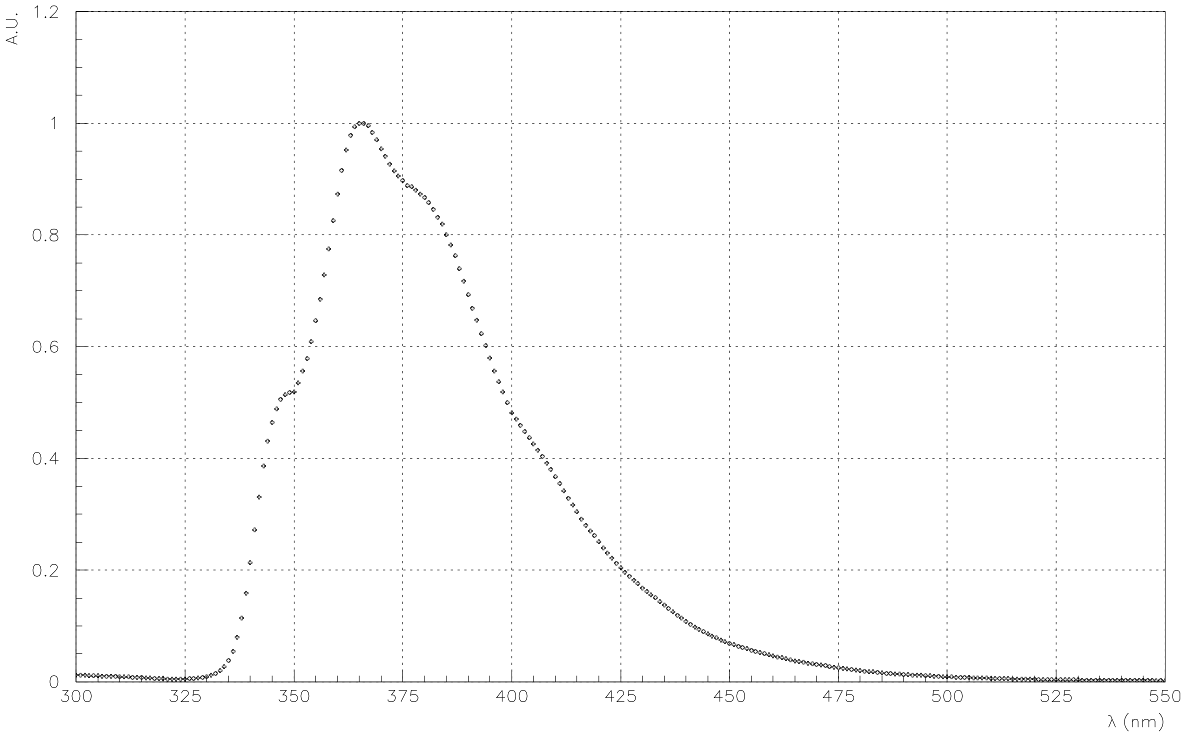
A.U.
1.2
1
0.8
0.6
0.4
0.2
0
300
325
350
375
400
425
450
475
500
525
550
λ (nm)

Figure 1:

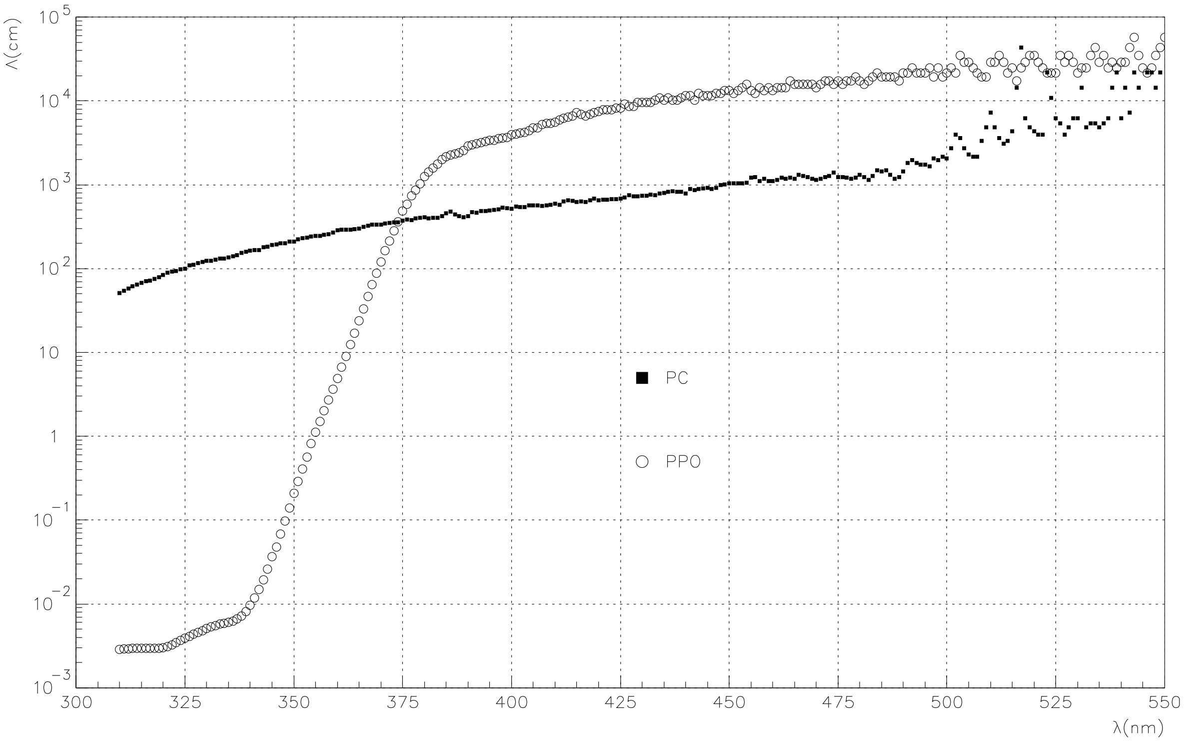

Λ(cm)
10^5
10^4
10^3
10^2
10
1
10^-1
10^-2
10^-3
300
325
350
375
400
425
450
475
500
525
550
λ(nm)
PC
PPO

Figure 2:

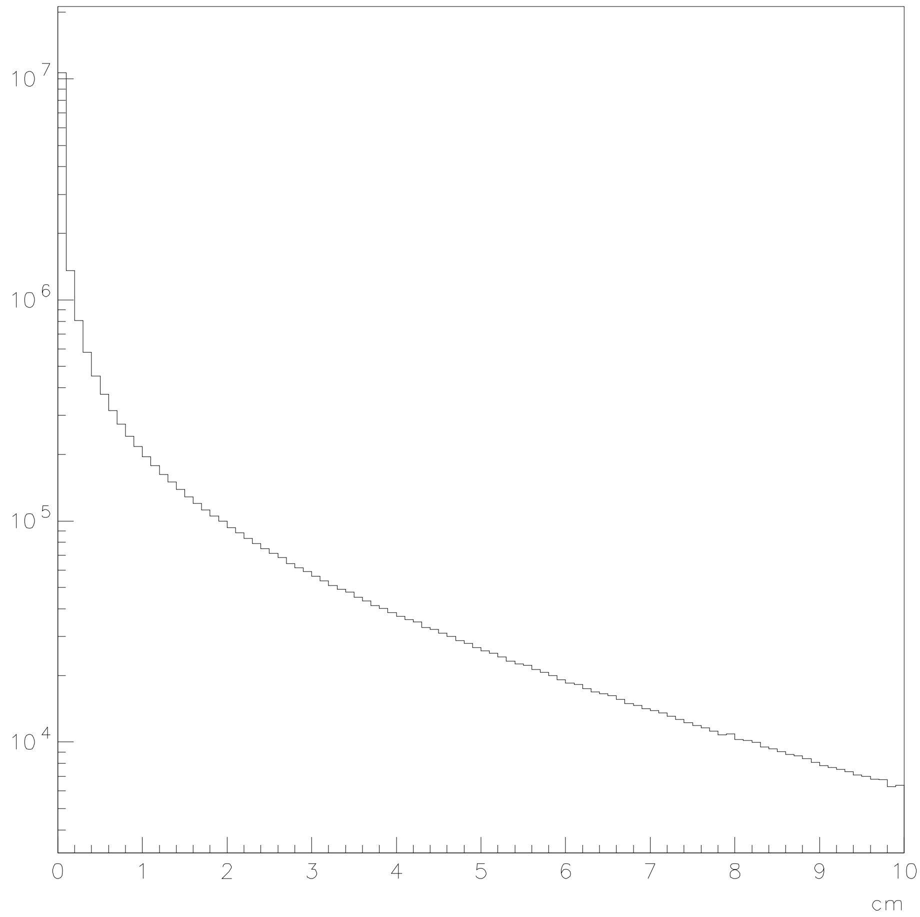

Figure 3:

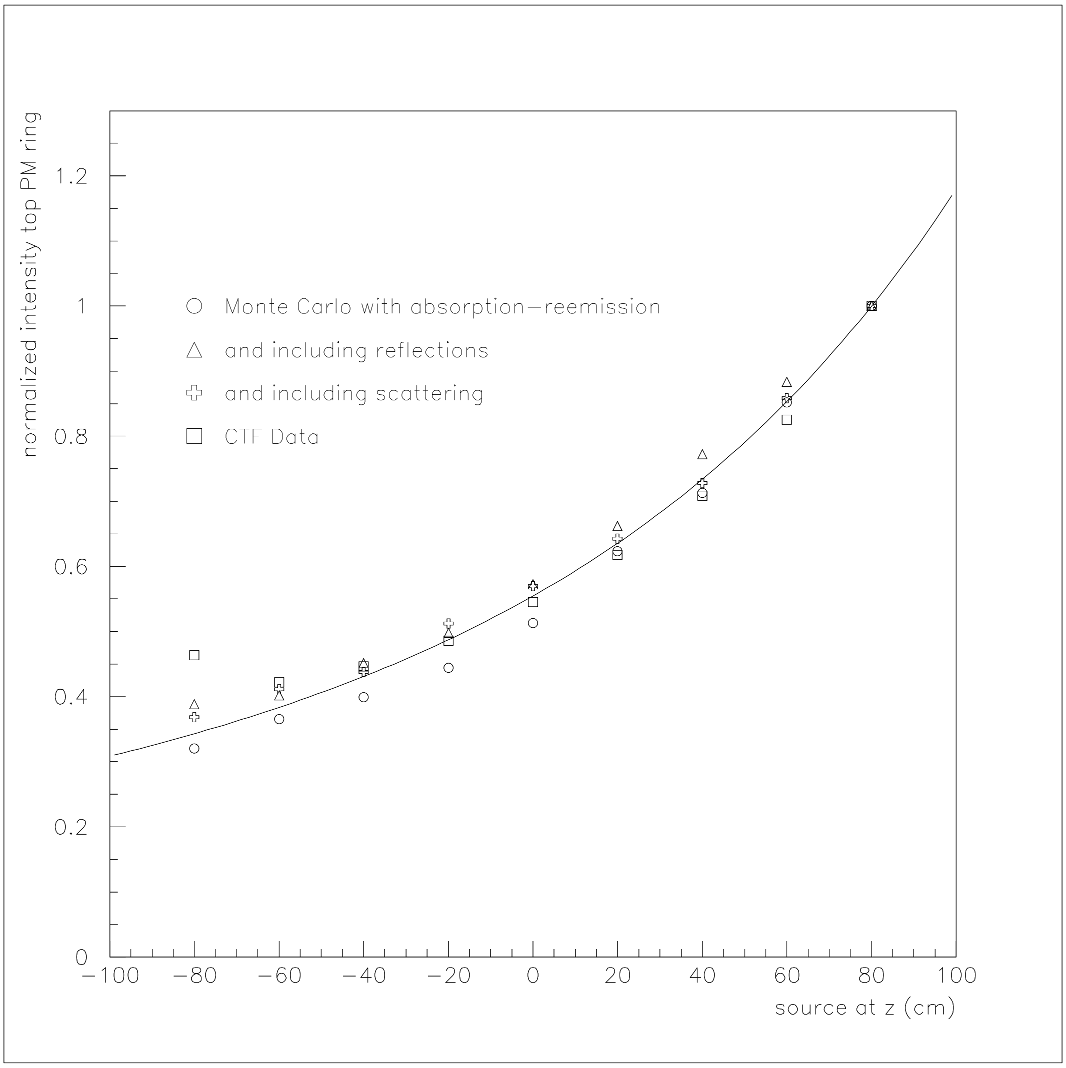
normalized intensity top PM ring
source at z (cm)
Monte Carlo with absorption−reemission
and including reflections
and including scattering
CTF Data
0
0.2
0.4
0.6
0.8
1
1.2
−100
−80
−60
−40
−20
0
20
40
60
80
100

Figure 4:

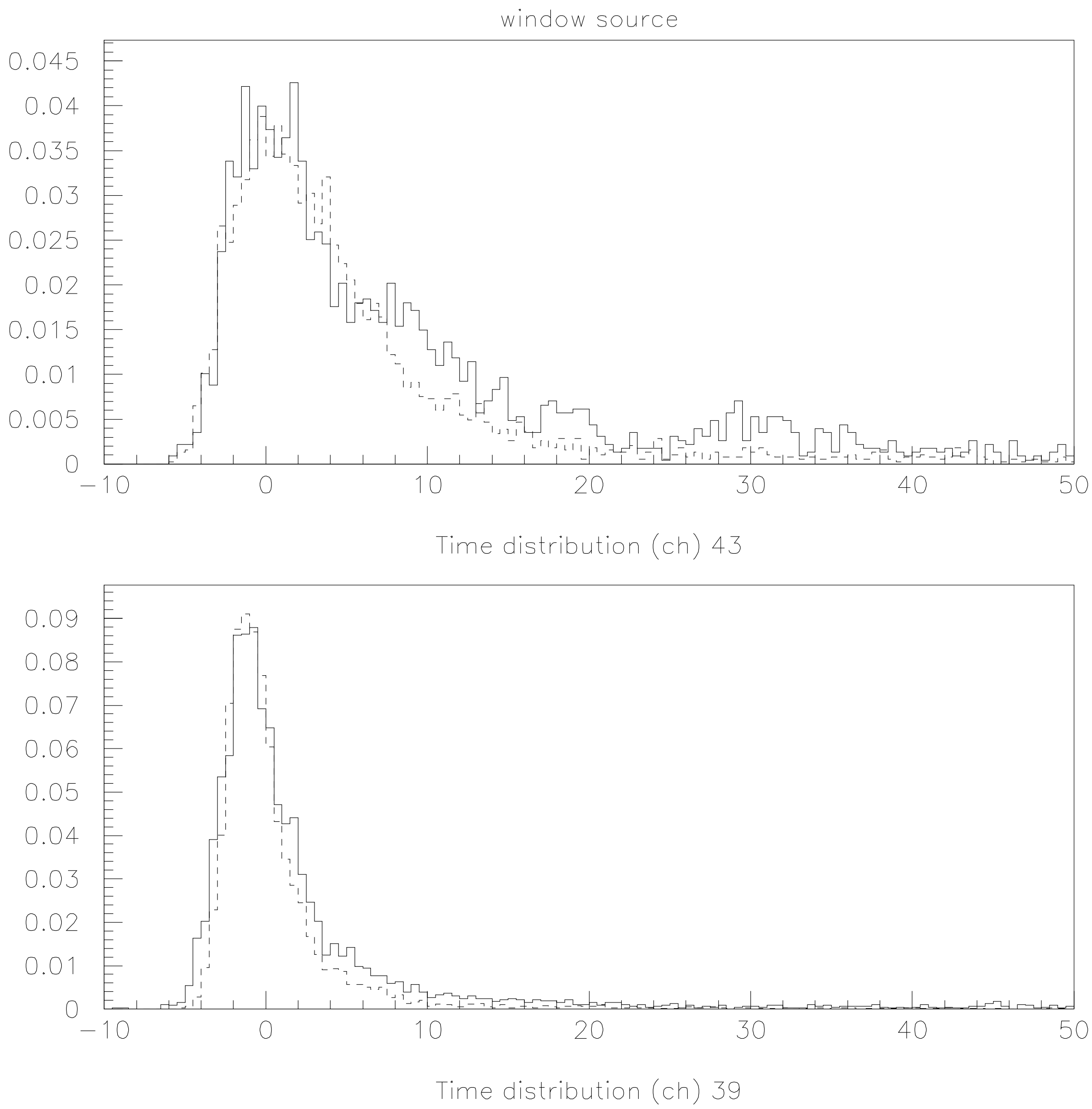
window source
0.045
0.04
0.035
0.03
0.025
0.02
0.015
0.01
0.005
0
−10
0
10
20
30
40
50
Time distribution (ch) 43
0.09
0.08
0.07
0.06
0.05
0.04
0.03
0.02
0.01
0
−10
0
10
20
30
40
50
Time distribution (ch) 39

Figure 5:

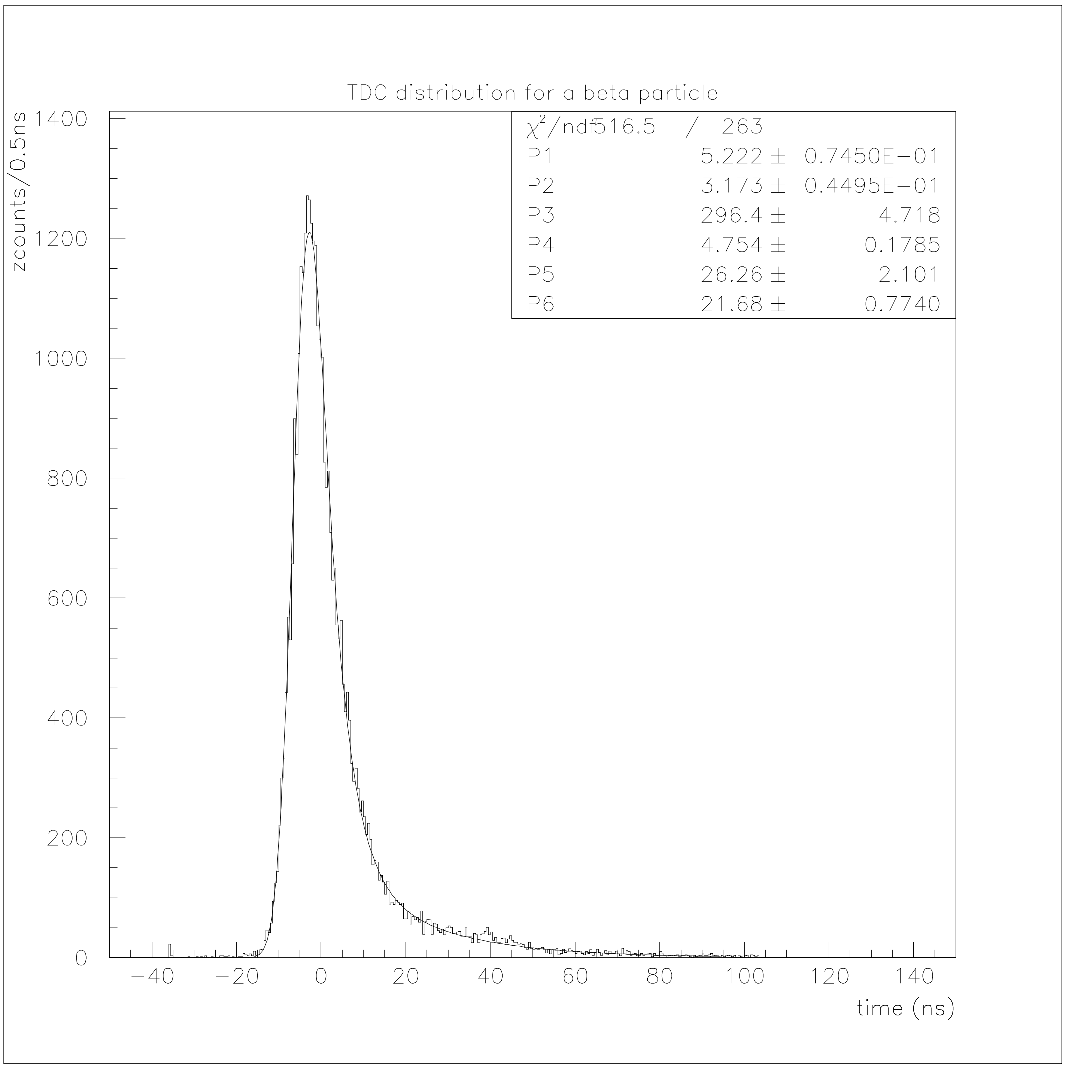
TDC distribution for a beta particle
zcounts/0.5ns
time (ns)
χ²/ndf 516.5 / 263
P1 5.222 ± 0.7450E-01
P2 3.173 ± 0.4495E-01
P3 296.4 ± 4.718
P4 4.754 ± 0.1785
P5 26.26 ± 2.101
P6 21.68 ± 0.7740
0
200
400
600
800
1000
1200
1400
−40
−20
0
20
40
60
80
100
120
140

Figure 6:

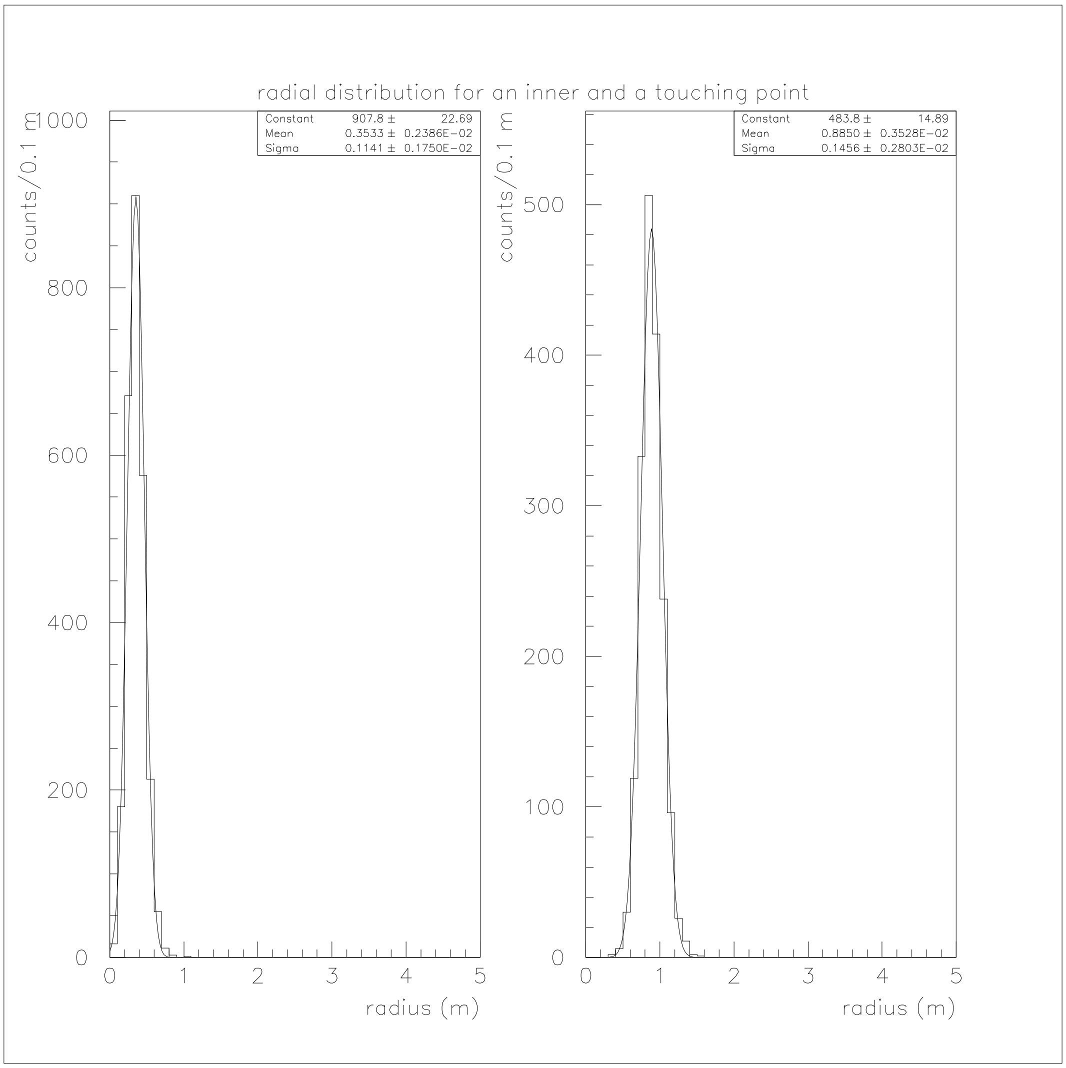
radial distribution for an inner and a touching point
Constant 907.8 ± 22.69
Mean 0.3533 ± 0.2386E-02
Sigma 0.1141 ± 0.1750E-02
counts/0.1 m
1000
800
600
400
200
0
0
1
2
3
4
5
radius (m)
Constant 483.8 ± 14.89
Mean 0.8850 ± 0.3528E-02
Sigma 0.1456 ± 0.2803E-02
counts/0.1 m
500
400
300
200
100
0
0
1
2
3
4
5
radius (m)

Figure 7: